# A Study on the Preparation of Polyester Thin Films for Use in Gas Detector Windows

Chun Li,[1] HengDong Wang,[2] YaoXiang Mo,[1] Qian Gong,[1] SuYong Hu,[1] and Li Shen[1,*]

[1]*Donghua University College of Chemistry and Chemical Engineering, Shanghai 201620, China*
[2]*Shanghai Institute of Applied Physics, Chinese Academy of Sciences, Shanghai 201800, China*

The thin window of a gas detector is crucial for allowing X-rays or other radiation to penetrate the detector. Today, the thin window at the entrance of the gas detector relies mainly on imports. The penetration performance of polyester films as incident windows for thin-window gas detectors was improved through the combination of plasma treatment and an organic-inorganic hybrid coating. Plasma modification provides an efficient way to achieve surface etching and polar group formation, therefore, the organic-inorganic hybrid coating fastness on the film could be efficiently increased. Scanning electron microscopy (SEM), Fourier transform infrared (FTIR), X-ray photoelectron spectroscopy (XPS), energy-dispersive X-ray spectroscopy (EDS), and contact angle measurements were employed to analyze the surface morphology, chemical composition, and hydrophilicity of the modified films. Experimental results revealed that increased plasma treatment power and duration improved surface roughness and hydrophilicity, and significantly improved coating adhesion and uniformity. X-ray fluorescence spectroscopy confirmed a marked reduction in particle loss, demonstrating the coating films' improved suitability for high-sensitivity particle detection applications. This approach shows potential for further optimization, offering a viable pathway to advance thin-window gas detector technologies.

Keywords: plasma treatment, thin window, gas detector, particle penetration efficiency

## 1. Introduction

Gas detectors primarily identify radiation or gas leaks by generating an electric charge or current through gas ionization. When an electric field is applied, positive ions and electrons produced by ionization move to the electrode, forming a current signal. This signal intensity is proportional to both the radiation intensity and the gas properties [1, 2]. Therefore, the radiation intensity entering the detector is critical for accurate measurements. Common types of gas detectors include ionization chambers, proportional counters, and Geiger-Muller counters, each of which optimizes detection sensitivity for specific radiation by using distinct gases and pressures [3]. Gas detectors are also employed to detect toxic and flammable gases in environments such as mines and industrial production [4–7]. The thin window of a gas detector is a crucial element, permitting X-rays or other radiation to penetrate the detector while minimizing energy absorption. To minimize radiation energy loss, the thin window facilitates the penetration of radiation into the detector, highlighting the critical importance of selecting appropriate window thickness and material properties [8]. Typically, materials such as polyester film, polypropylene film, beryllium, silicon nitride, and zinc oxide are used for thin Windows [9–12]. However, at present, such thin Windows are mainly dependent on imports, which presents challenges in terms of cost, accessibility, and sustainability.

There are two main directions to increase the particle penetration of the incident-thin window. The first approach involves making the film as thin as possible to reduce radiation or particle loss during penetration. For instance, Torma et al. [13] investigated the use of ultra-thin silicon nitride windows in soft X-ray detection, finding that this material's transmittance under low-energy X-rays surpasses that of existing technologies. Segal et al. [14] introduced a microwave annealing technique to manufacture ultra-thin incident windows, which enables dopant activation at low substrate temperatures, minimizing diffusion issues and achieving an exceptionally thin window to boost efficiency. The second approach applies an anti-reflective coating to the film surface, using materials with low atomic numbers, low electron cloud density, and low refractive index to reduce reflection, scattering, and absorption at the film interface. Li et al. [15] employed low-refractive index coatings like $TiO_2$ and $Al_2O_3$ to create multilayer anti-reflective films with excellent transmittance. Lemarquis et al. [16] used $SiO_2$ for anti-reflective coating, leveraging its low refractive index to produce films with high transmittance in the visible, near-infrared, and mid-infrared ranges. Selecting low atomic number materials as anti-reflective coatings effectively minimizes reflection and scattering, improving transmittance since these materials' sparse electron clouds result in weak interactions with rays or particles, allowing particles to pass through the film more easily.

Polyester film is one of the traditional thin window materials due to its excellent mechanical properties, chemical tolerance, and cost effectiveness [17–19]. The main method of modification is to make it thinner, but its effect is often poor when measuring low-energy heavy ions [20, 21]. Besides, polyester can be coated and modified to reduce scattering and energy loss during penetration for higher precision testing. Unmodified polyester films have hydrophobicity and smooth surfaces, which significantly impede their adhesion to coatings. Coatings are critical for enhancing particle transmittance and minimizing scattering losses, and these limitations restrict the direct application of polyester films in high-precision gas detectors.

Surface modification techniques offer effective solutions to address the challenges associated with polymer materials, particularly improving surface properties. Among these, plasma treatment has emerged as a widely employed method

* Corresponding author, Li Shen, Donghua University College of Chemistry and Chemical Engineering, 13918195849, shenli@dhu.edu.cn

due to its ability to introduce polar functional groups on polymer surfaces [22]. For instance, Yang et al. utilized anhydrous ammonia plasma treatment to modify polylactic acid (PLA) films, introducing oxygen- and nitrogen-containing functional groups on the surface [23]. This modification significantly enhanced the hydrophilicity and cellular adhesion properties of the films. Similarly, Casimiro et al. investigated the use of ammonia or ammonia-hydrogen plasma treatments to introduce amino groups onto polyethylene terephthalate (PET) films [24]. Their study focused on changes in surface chemical composition and hydrophilicity stability, demonstrating that surfaces treated with ammonia plasma exhibited superior stability over time. This modification can improve the hydrophilicity of mylar, creating an active site for subsequent coating applications. Organic-inorganic hybrid coatings are widely used in film modification because they combine the flexibility of organic polymers with the durability and functionality of inorganic materials. For instance, Zheng et al. explored the application of sol-gel hybrid coatings in metal corrosion protection, highlighting their ability to improve adhesion between the coating and substrate through chemical bonding while simultaneously optimizing surface functional propertiess [25]. Similarly, Iotti et al. investigated coatings based on organic-inorganic hybrid materials, such as siloxanes and polylactic acid (PLA), and demonstrated their effectiveness in improving oxygen and water vapor barrier properties [26]. Additionally, these coatings enhanced the uniformity and adhesion of the film.

The purpose of this research is to promote the development of the domestic incidence thin window of gas detectors and expand its application in the field of high precision. In this study, the polyester surface of a single-sided aluminum-plated polyester film was plasma-treated to enhance hydrophilicity, and gamma rays were used to prepare an adhesive and create an organic-inorganic hybrid material comprising methacrylic acid, nano-$SiO_2$, and other components. These materials were combined to form an anti-reflective coating liquid, which was then applied to the polyester surface. The coating's effectiveness was characterized by FTIR, SEM, XPS, EDS, and contact angle analysis, while coating stability was assessed through weight gain rate and coating fastness tests. Additionally, particle penetration loss improvement was measured using an X-ray fluorescence spectrometer.

# 2. Materials and methods

## 2.1. Materials

Single-sided aluminum-plated polyester film (commercially available, thickness 8$\mu$m); methacrylic acid, potassium persulfate, methyl methacrylate, silane coupling agent, ethylene glycol dimethacrylate, polyethylene glycol 1000, the above reagents were purchased from Shanghai Aladdin Biochemical Technology Co., Ltd.; nano-$SiO_2$, anhydrous ethanol, were obtained from Sinopharm Chemical Reagent Co., Ltd.; sodium carboxymethyl cellulose, acrylic acid, deionized water, the above reagents were gotten from Shanghai Shilong Technology Co., Ltd.

## 2.2. Preparation of the adhesive

To prepare the adhesive, 22 g of anhydrous ethanol was added to 8 g sodium carboxymethyl cellulose, followed by the addition of 338 g of deionized water. The mixture was stirred with an electric mixer for 15 minutes, during which a blend of 24 g of acrylic acid and 8 g of methyl methacrylate was gradually introduced. The prepared solution was then subjected to vacuum treatment, followed by nitrogen purging. The sealed solution was placed in an ultrasonic oscillator for three 15-minute cycles. Finally, the solution was irradiated in a $^{60}$Co-$\gamma$ ray chamber (Shanghai Shilong Technology Co., Ltd.) for 24 hours to yield the final adhesive.

## 2.3. Preparation of the organic-inorganic hybrid coating solution

10 g of $SiO_2$ nanoparticles were dispersed in 190 mL of water to form a 5 wt% $SiO_2$ dispersion. A 0.1 mL silane coupling agent was added to the $SiO_2$ dispersion system, and the mixture was stirred at 70°C for 30 minutes. Subsequently, a solution containing 5 mL of methacrylic acid, 5 mL of ethylene glycol dimethacrylate, and 5 g of polyethylene glycol 1000 was added dropwise to the system under continuous stirring. The reaction was initiated by an aqueous solution of potassium persulfate ($K_2S_2O_8$). The resulting solution was diluted to a concentration of 5 wt% using an ethanol-water mixture with a 1:1 volume ratio, then combined with the homemade adhesive to obtain the final organic-inorganic hybrid coating solution.

## 2.4. Preparation of the modified films under different conditions

The base film was cut into dimensions of 10 cm $\times$ 10 cm. One side of the polyester surface of the metalized polyester film was treated using a plasma treatment device (Europlasma, Belgium), with treatment parameters set to power levels ranging from 0 to 200 W and treatment times ranging from 0 to 5 minutes. A specific amount of coating solution, with adhesive content varying from 0 to 70 wt%, was applied onto the base film surface using a scraper. The coated film was then dried at 80°C for 60 minutes.

## 2.5. Fourier transform infrared spectroscopy (FTIR)

Fourier transform infrared spectroscopy (FTIR) with attenuated total reflectance mode (A7440GP, Bont Instrument Co., Sweden) was used to characterize the film before and after modification. The resolution was set to 2 $cm^{-1}$, with a scanning range of 400$cm^{-1}$-4000 $cm^{-1}$.

### 2.6. Scanning electron microscopy (SEM)

A scanning electron microscope (SEM S-4800, Hitachi Analytical Instruments Co.) was employed to observe the microstructure of the modified film's surface.

### 2.7. Contact angle measurement

To evaluate the hydrophilic performance of the modified film, a droplet of 8 microlitre of water was deposited onto the film surface, and the contact angle was measured after 10 seconds. The contact angle (ThetaLite,Biolin Scientific AB) was measured at five different positions on the film surface, and the average value was recorded.

### 2.8. Weight gain rate (W)

The weight gain rate of the film was calculated based on the mass difference before and after coating, using the following formula:

$$W = \frac{m_1 - m_0}{m_0} \times 100\% \tag{1}$$

where $m_0$ is the mass before coating, and $m_1$ is the mass after coating.

### 2.9. Particle transmission loss improvement rate (I)

The improvement rate of particle transmission loss was determined by measuring the difference in particle transmission loss between the original film and the modified film using X-ray fluorescence spectroscopy (XRF930 Plating Thickness Gauge,Shanghai Institute of Applied Physics, Chinese Academy of Sciences). The rate was calculated using the following formula:

$$I = \frac{n_0 - n_1}{n_0} \times 100\% \tag{2}$$

where $n_0$ is the particle loss during X-ray transmission through the original film, and $n_1$ is the particle loss through the modified film.

### 2.10. X-ray Photoelectron Spectroscopy (XPS)

An X-ray photoelectron spectrometer (Thermo ESCALAB 250X, Dalian Institute of Chemical Physics, Chinese Academy of Sciences) was utilized to analyze the elemental composition and valence states on the film surface before and after coating.

### 2.11. Energy-Dispersive Spectroscopy (EDS)

EDS (X-MaxN 80T, Oxford Instruments) mapping was performed using a field emission scanning electron microscope to obtain elemental spectra and distribution maps of the film after coating.

### 2.12. Reduction rate of coating quality (Q)

To evaluate coating durability, the coated film was washed according to GB/T 3921–2008 "Textiles Tests for Color Fastness—Color Fastness to Washing" method. The reduction rate of coating quality was recorded before washing ($l_1$) and after washing ($l_2$), and The reduction rate of coating quality was calculated as follows:

$$Q = \frac{l_1 - l_2}{l_1} \times 100\% \tag{3}$$

## 3. Results and discussion

### 3.1. Analysis of plasma etching effect on film surface

Plasma treatment induces changes in the surface properties of polyester films through the bombardment of high-energy particles and chemical reactions. The high-energy electrons, ions, and free radicals in the plasma can etch the film's surface and introduce polar groups.

Fig. 1 illustrates that the untreated polyester film surface is smooth, limiting its adhesion to coatings. Plasma modification is weak at lower power levels, resulting in minimal etching. However, the polyester film exhibits pronounced etching effects when the power is increased to 200W, such as fine pits or cracks, which contribute to increased surface roughness compared to the untreated film. Extending plasma treatment time to 4 minutes further amplifies etching and surface roughness, with a notable increase in the number and depth of etching pits compared to 2 minutes of treatment.

### 3.2. Test of contact angle and weight gain rate of modified film

As shown in Fig. 2(a)and Fig. 2(c), an increase in plasma treatment time and power reduces the contact angle of the coated film. This reduction occurs due to the generation of free radicals and polar groups on the film surface during plasma treatment, which can stimulate molecular restructuring, break chemical bonds, and create active sites [27–30].

Meanwhile, as illustrated in Fig. 2(b) and Fig. 2(d), increased plasma treatment time and power also elevate the weight gain rate. The active sites generated during plasma treatment provide additional bonding points for the coating, while the etching process increases surface roughness, thereby expanding the contact area. This enhanced surface structure allows the coating liquid to distribute and adhere more effectively, significantly improving the stability and uniformity of the coating.

Thus, as processing time and power increase, the film surface becomes more reactive, leading to a steady increase in the amount of coating that adheres to it. However, the figure shows that after reaching 5 minutes, the weight gain rate begins to plateau, likely due to surface saturation. Prolonged plasma treatment can also excessively etch the film, compromising its mechanical properties and introducing an excessive

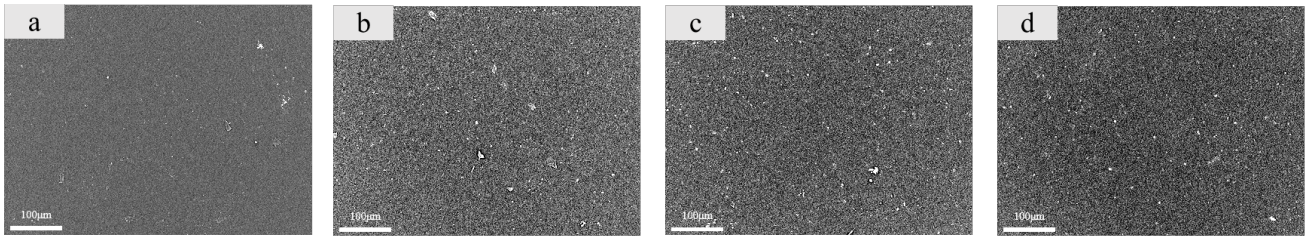


Fig. 1. SEM images of the uncoated original film and the uncoated modified base film under different plasma treatment conditions a: original film; b: 2min+50W; c: 2min+200W; d: 4min+200W

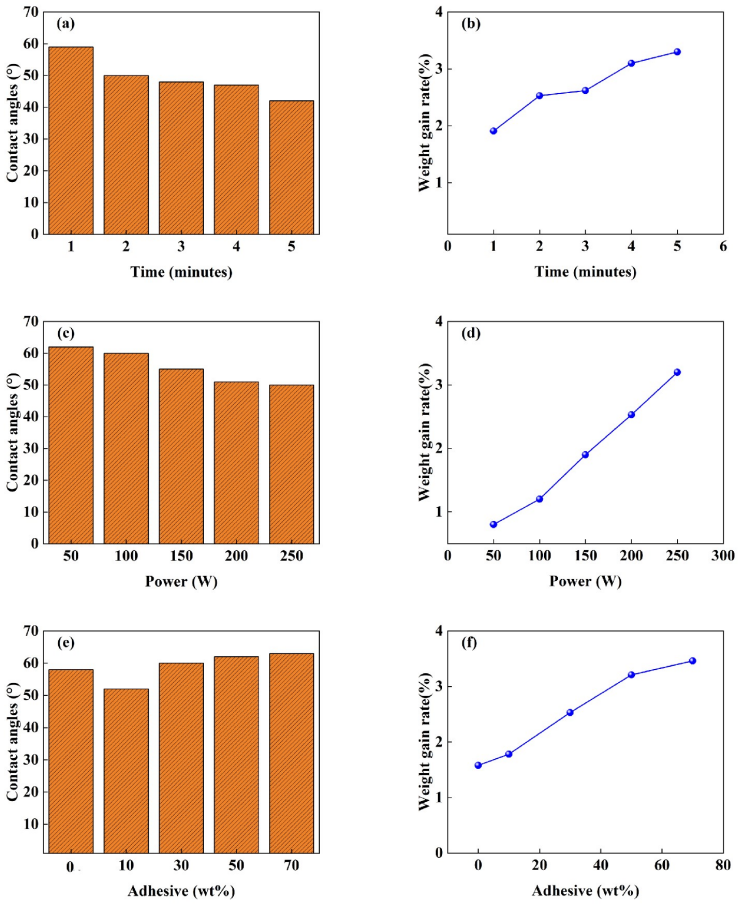


Fig. 2. Effect of different plasma treatment conditions on contact angle and weight gain rate of coated films: (a) Effect of different plasma treatment time on contact angle; (b) Effect of different plasma treatment time on weight gain rate; (c) Effect of different plasma treatment power on contact angle; (d) Effect of different plasma treatment power on weight gain rate; (e) Effect of different adhesive dosages on contact angle; (f) Effect of different adhesive dosages on weight gain rate.

number of reactive sites, which can lead to overly thick coatings that reduce uniformity and promote clustering. Therefore, optimal plasma treatment conditions must balance treatment parameters, weight gain, and contact angle to achieve desirable results.

As shown in Fig. 2(e), the contact angle exhibited a U-shaped trend. Under low-adhesive conditions, the adhesive and solution combine well, producing a uniform, well-covered coating that enhances surface hydrophilicity. Plasma treatment further reduces the contact angle by enabling a low adhesive concentration to promote even coating distribution without adverse surface effects. However, as adhesive concentration reaches 50 wt%, the contact angle increases, likely due to reduced coating uniformity from thicker coatings and clustering. To achieve optimal coating, adhesive dosage must be carefully managed to balance adhesion and hydrophilicity.

Fig. 2(f) shows that the weight gain rate rises with the adhesive amount. The primary role of adhesive is to enhance coating-substrate adhesion; optimal adhesive concentrations facilitate film adherence. At higher adhesive concentrations, the weight gain rate increases more rapidly due to enhanced coating thickness and improved adhesion between the coating and the film surface. Excessive adhesive can lead to an overly thick coating, reducing uniformity and causing clusters that may increase particle scattering. Thus, adhesive dosage should balance adhesion and thickness control, optimizing coating uniformity and stability.

## 3.3. Coating fastness test

Fig. 3 illustrates the effects of plasma treatment time (a), power (b), and adhesive dosage (c) on the coating fastness of the modified film. As plasma treatment time increased from 0 to 5 minutes and power increased from 0 W to 250 W, the rate of coating quality reduction steadily decreased, with the untreated base film showing the highest reduction rate. This indicates that plasma treatment enhances coating fastness. Combined with the contact angle test results, the findings suggest that an increase in polar groups provides more active sites, improving the film's hydrophilicity. Plasma etching also roughens the film surface, increasing the contact area with the coating solution and thereby enhancing coating fastness.

Adhesive dosage significantly affects coating fastness as well. Without adhesive, the reduction rate is highest; however, with 10 wt% adhesive, the degradation rate decreases notably. When the adhesive dosage further increases to 50 wt% and 70 wt%, the reduction rate increases again. This may be due to an excessive adhesive amount diminishing surface properties and weakening coating adhesion.

Overall, suitable plasma treatment and adhesive dosages are essential to achieving coating stability.

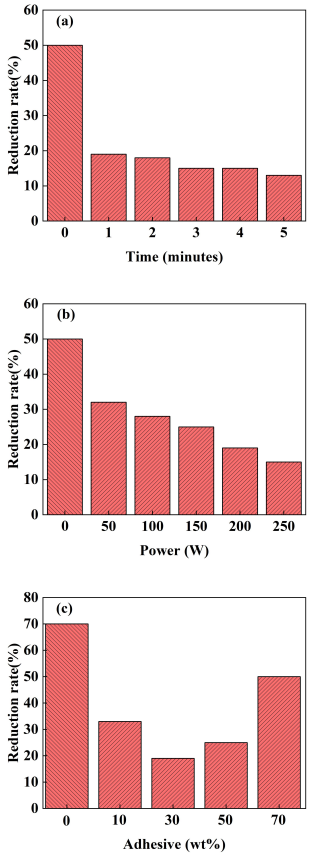


Fig. 3. Reduction rate of coating quality after film cleaning under different treatment conditions a: time; b: power; c: adhesive dosage

## 3.4. Analysis of micromorphology of modified films

The SEM images reveal the micromorphology of polyester films Fig. 4 subjected to different plasma treatment durations, powers, and adhesive concentrations. The original film (a) displays a smooth and featureless surface, characteristic of untreated polyester, which lacks active sites for coating adhesion. This absence of surface roughness limits coating adherence, resulting in poor uniformity when a coating is applied. After 1 minute of plasma treatment at 200W with a 30 wt% adhesive concentration (b), the surface begins to exhibit subtle texturing, with minor etching visible. The coating distribution improves compared to the original film, but the limited plasma exposure time results in insufficient surface roughness to enable complete and uniform coating coverage.

When the plasma treatment duration is increased to 2 minutes under the same conditions (c), the film surface shows more pronounced etching. This enhanced microstructure creates additional active sites, resulting in a more uniform coating. The distribution is improved, and surface coverage increases, indicating that the extended plasma treatment effectively enhances the interaction between the film surface and the coating material. However, at 3 minutes of plasma treatment (d), although the etching is further intensified, leading to greater coating material coverage, areas of particle aggregation start to appear. This suggests that prolonged plasma exposure can create excessive roughness, disrupting the uniformity of the coating .

The effect of plasma power is evident when comparing the films treated at 50W (e) and 250W (f) for 2 minutes, both with 30 wt% adhesive. At the lower power of 50W, the surface etching is minimal, leading to a relatively smooth surface with sparse and uneven coating distribution. The lower energy input is insufficient to create a significant number of active sites, resulting in weaker adhesion and less effective coating. Conversely, at 250W, the plasma treatment induces severe surface roughness and extensive etching. Although this will produce a large number of active sites, with the increase of the amount of coating on the surface of the film, part of the coating liquid on the surface of the film will accumulate, resulting in uneven coating.

The influence of adhesive concentration is showed by comparing films with 10 wt% (g) and 70 wt% (h) adhesive, both treated for 2 minutes at 200W. At 10 wt%, the coating is sparse and poorly distributed, as the limited adhesive content cannot provide sufficient material to uniformly cover the surface, even with plasma-induced active sites. In contrast, at 70 wt%, the excessive adhesive leads to thick coatings with significant particle aggregation. The surface is densely covered but lacks uniformity, with large clusters disrupting the coating's evenness. This highlights the importance of optimizing adhesive concentration to balance coverage and uniformity without overloading the surface with excess material.

Overall, the analysis underscores the complex interplay between plasma treatment parameters and adhesive concentration. Moderate plasma power (200W) and treatment duration (2 minutes) combined with an optimal adhesive concentration

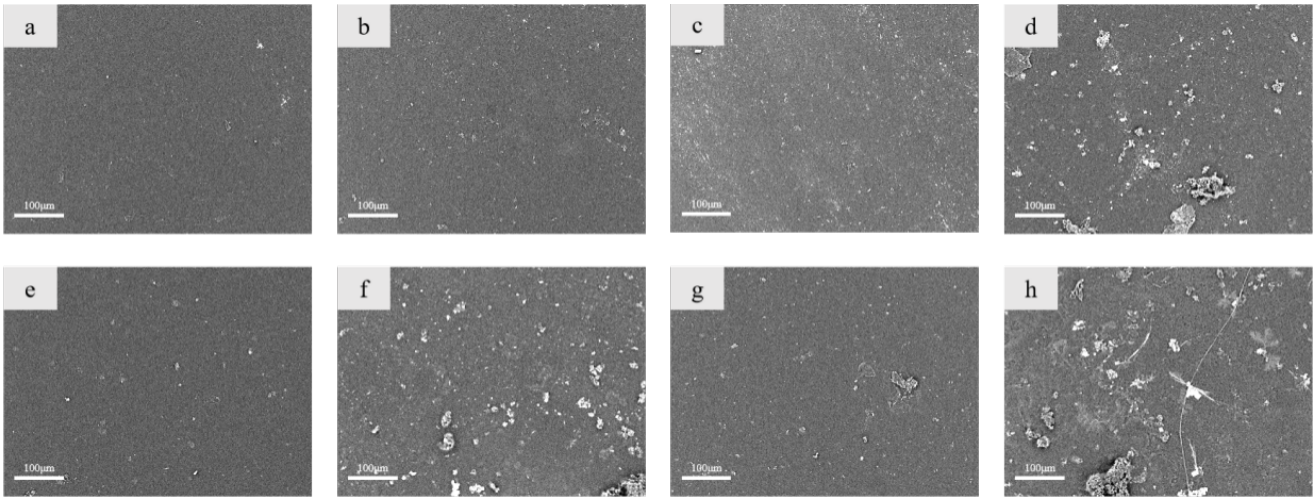


Fig. 4. SEM images of the surfaces of the coated modified films under different plasma treatment and adhesive conditions: (a) original film; (b) 1 min, 200 W, 30 wt%; (c) 2 min, 200 W, 30 wt%; (d) 3 min, 200 W, 30 wt%; (e) 2 min, 50 W, 30 wt%; (f) 2 min, 250 W, 30 wt%; (g) 2 min, 200 W, 10 wt%; (h) 2 min, 200 W, 70 wt%.

result in the most uniform and well-adhered coatings. Excessive plasma power or adhesive concentration leads to non-uniformity due to over-etching or material aggregation, while insufficient plasma power or adhesive concentration yields sparse and uneven coatings.

## 3.5. Infrared spectrum analysis of modified films

Fig. 5 presents the infrared spectra of modified films under varying conditions. The C=O stretching vibration peak of the unmodified PET film appears at 1722 $cm^{-1}$. After coating, this peak intensifies due to the presence of methacrylic acid and ethylene glycol dimethacrylate in the coating liquid, which also contains C=O groups. Absorption peaks at 1581 $cm^{-1}$ and 1482 $cm^{-1}$ likely originate from the adhesive, specifically the $COO^-$ groups in sodium carboxymethylcellulose. The antisymmetric $COO^-$ stretching vibration appears at 1581 $cm^{-1}$, while the symmetric vibration appears at 1482 $cm^{-1}$. Additionally, the 1087 $cm^{-1}$ peak results from the nano-$SiO_2$ in the coating, corresponding to the Si-O-Si stretching vibration, confirming the coating material's presence on the film surface.

## 3.6. EDS analysis of modified films

EDS surface scan data in Fig. 6 confirms the presence of organic-inorganic hybrid materials in the coating. Sodium is sourced from sodium carboxymethyl cellulose and silicon from nano-SiO2. Sodium signals are prominent due to uniform adhesive dispersion, resulting in even sodium distribution in the coating. Although silicon signals are weaker, they are uniformly distributed, indicating nano-silica's even dispersion within the coating. Uniformly dispersed silicon contributes to the improvement of the coating's anti-reflective properties; however, excessive nano-SiO2 content

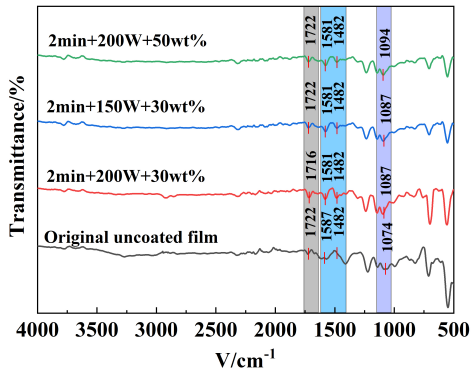


Fig. 5. Infrared spectra of modified films under different conditions

could cause aggregation, impairing film performance.

## 3.7. XPS test of modified films

XPS energy spectrum data in Fig. 7 shows chemical composition changes in the polyester film before and after coating with an organic-inorganic hybrid material. The full spectrum in Figure 9(a) reveals the elemental peaks of the original and coated films, with the original film showing only oxygen (O1s), carbon (C1s), and silicon (Si2p) peaks. After coating, a new sodium (Na1s) peak appears, indicating the presence of sodium carboxymethyl cellulose in the adhesive. Fig. 7(b) and Fig. 7(c) depict carbon spectra of the original and coated films, respectively. The original film's carbon spectrum primarily shows C=C (284.8 eV), C-O (286.4 eV), and O-C=O (288.9 eV), while the coated film introduces new C-H (285.7 eV), C=O (289.7 eV), and C-C (284.1 eV) peaks, confirming the application of organic coating components.

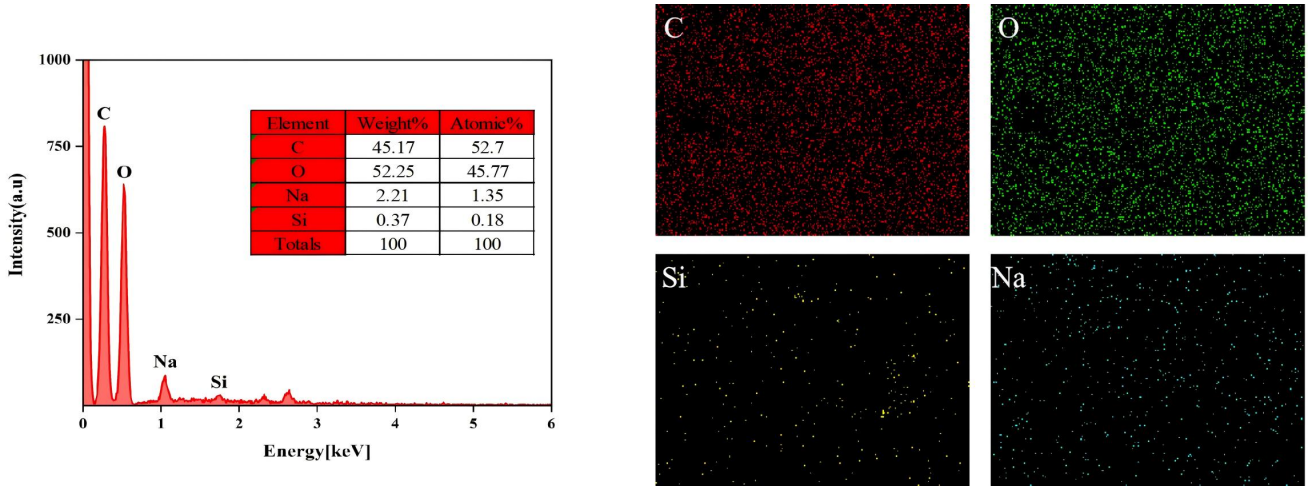


Fig. 6. EDS energy spectrum and element distribution diagram of modified film a: energy spectrum; b: element distribution diagram

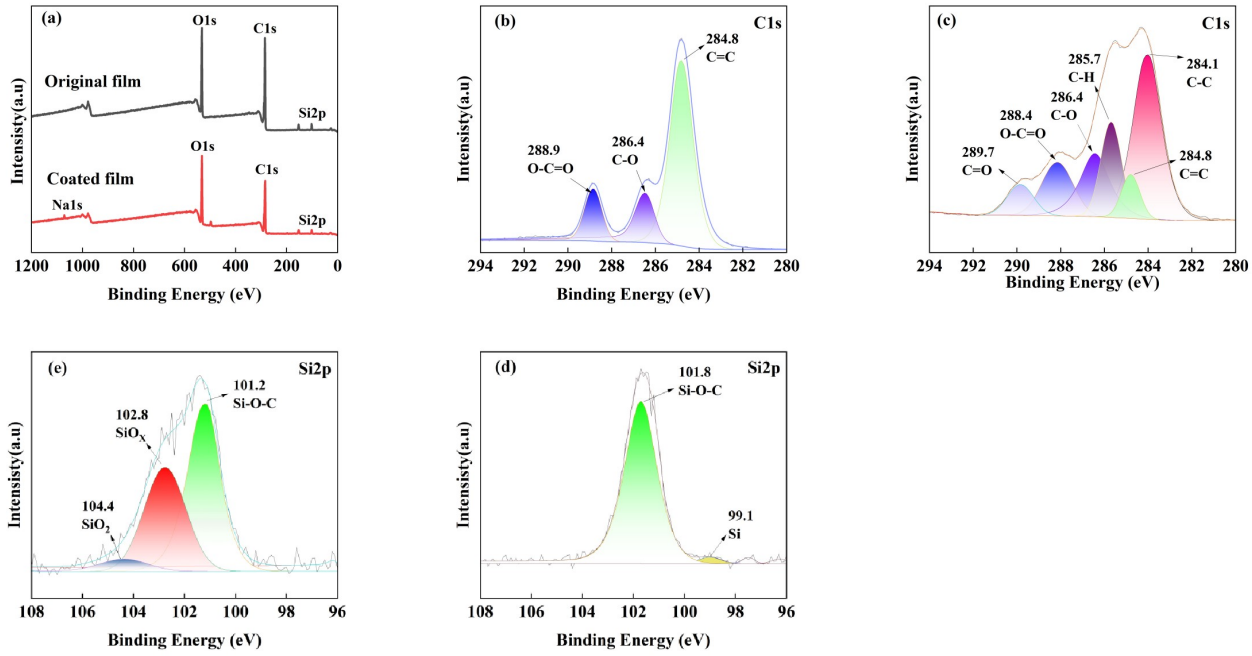


Fig. 7. XPS energy spectrum of the base film and modified film a: full spectrum of the original film and modified film; b: carbon spectrum of the base film; c: carbon spectrum of the modified film; d: silicon spectrum of the base film; d: silicon spectrum of modified film

## 3.8. Particle penetration test

Fig. 8(a) indicates that the particle loss improvement rate initially rises with increasing plasma time but subsequently declines. At 1 to 2 minutes of treatment, polar groups and etching effects promote a more even distribution of coating material. As long as coating thickness does not affect penetration, the coating material reduces energy loss and particle scattering, thus improving penetration rates. However, prolonged treatment leads to over-etching or coating material aggregation, reducing coating uniformity and increasing particle scattering and absorption. Fig. 8(b) reveals an initial increase, followed by a decrease, in particle loss improvement rate as plasma power increases. At 200 W, optimal particle loss improvement is achieved, suggesting optimal coating structure modification. However, excessively high power (250 W) can lead to over-etching or overly thick coatings, compromising uniformity and increasing particle scattering and absorption. Fig. 8(c) illustrates that adhesive dosage significantly influences particle loss improvement. At 30 wt%, the improvement rate is maximized, whereas 10 wt% and 70 wt% result in lower rates. An optimal adhesive amount facilitates uniform coating distribution. Low adhesive concentration (10 wt%) yields sparse coverage, insufficient for an effective anti-

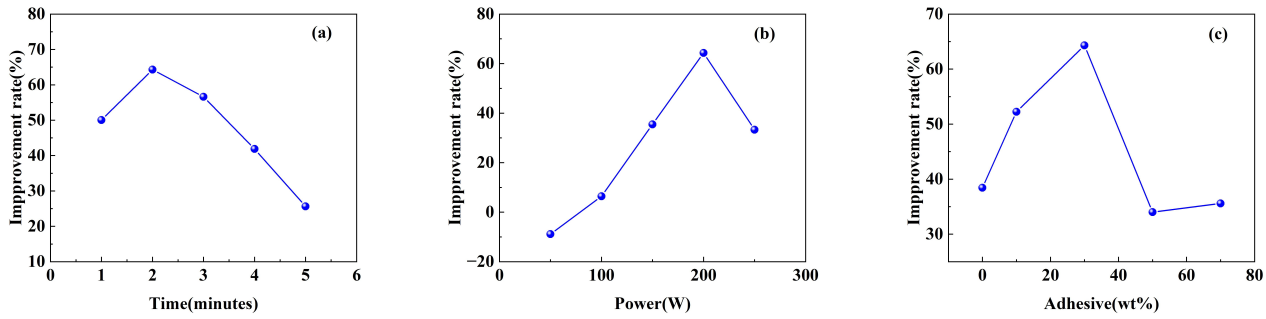


Fig. 8. Effect of different variables on the improvement rate of modified film particle loss a: plasma treatment time: b: plasma treatment power: c: adhesive dosage

reflective coating. In contrast, high concentration (70 wt%) results in thick coatings that increase scattering and absorption, thus reducing particle loss improvement.

### 3.9. Coating suitability analysis

The applicability of the organic-inorganic hybrid coating was further evaluated by analyzing its effectiveness on films of varying thickness and composition, including 6 $\mu$m, 8 $\mu$m, and 10 $\mu$m aluminum-coated films, as well as 12 $\mu$m transparent polyester films. The particle loss improvement rate, as depicted Fig. 9, demonstrates a strong enhancement for the aluminum-coated films with thicknesses of 6 $\mu$m, 8 $\mu$m, and 10 $\mu$m, reaching approximately 60%. This significant improvement indicates that the coating effectively reduces particle scattering and energy loss during transmission. In contrast, the particle loss improvement rate for the 12 $\mu$m transparent polyester film was markedly lower, at approximately 30%. This decline in performance can be attributed to the increased thickness of the transparent film, which inherently leads to greater energy loss during particle transmission. Additionally, the distinct surface characteristics of the transparent polyester film, such as its refractive index and surface interaction with the coating, may result in less effective adhesion and reduced functionality of the hybrid coating. The discrepancy underscores the influence of substrate material and thickness on the coating's performance.

These results highlight the coating's robust effectiveness in improving particle penetration for thin aluminum-coated films, while also indicating its moderate applicability for thicker, transparent substrates. The findings provide critical insights into the interplay between substrate characteristics and coating performance, offering a valuable framework for optimizing coating formulations and application parameters for specific film types. Future studies may focus on tailoring the coating composition to enhance its interaction with transparent substrates, thereby further broadening its applicability across diverse film materials and thicknesses.

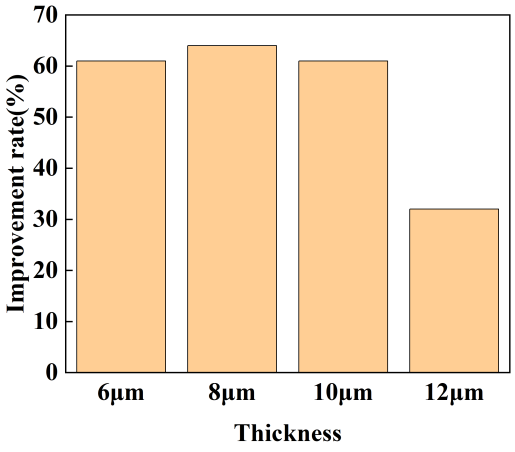


Fig. 9. Particle loss improvement rates of modified films with different thicknesses

## 4. Conclusions

The developed plasma treatment and organic-inorganic hybrid coating technique demonstrate a promising advancement in the preparation of thin-window gas detector films. Plasma treatment settings, such as power and duration, were found to significantly influence the film's surface characteristics, enhancing adhesion and hydrophilicity, which are critical for effective coating application. By adjusting the adhesive concentration, the study achieved optimal contact angles and weight gain rates, ensuring stable and uniform coatings that improve particle penetration and reduce scattering losses. Furthermore, the coating demonstrated broad applicability across films of varying thicknesses and compositions, with particularly notable improvements in particle penetration for aluminized polyester film. Even on thicker substrates, such as transparent polyester films, the coating achieved measurable enhancement, highlighting its adaptability for a wide range of film types and thicknesses. These findings position the modified films as highly effective for detecting low-energy X-rays and particles, emphasizing their potential utility in high-

sensitivity applications. Future research could build upon this work by exploring alternative coating compositions and advanced plasma treatment methods to further improve detector penetration efficiency, coating durability, and applicability across diverse materials and use cases.

# 5. References


[1] P. Gasik, M. Ball, L. Fabbietti, B. Ketzer, J. Margutti, A. Mathis, S. Weber, Discharge probability studies with GEM detectors. GSI Scientific Report 2013, 63 (2014).

[2] H. Liu, W. Zhu, Y. Han, Z. Yang, Y. Huang, Single-Nanowire fuse for ionization gas detection. Sensors, **19**(20), 4358 (2019).

[3] A. Melnikov, S. Gavrilov, Operation experience of ionization-proportional chamber for low-current beam measurements at INR RAS proton linac. Journal of Instrumentation, **15**(09), P09005 (2020).

[4] V. Sharma, Taksh, K. Srivastav, Priyam, N.A. Siddiqui, A critical study on role of sensor-based electronic system for toxic gas identification in the mining (coal) industry. Intelligent Communication, Control and Devices: Proceedings of ICICCD 2017, 1511–1521 (2018).

[5] R.K. Dwibedi, V. Vanitha, R.D. Sagar, P. PhaniSai, *et al*., Automatic gas leakage detection using IoT. IOP Conference Series: Materials Science and Engineering, **981**(4), 042085 (2020).

[6] A.J. Benavides-Serrano, M.S. Mannan, C.D. Laird, A quantitative assessment on the placement practices of gas detectors in the process industries. Journal of Loss Prevention in the Process Industries, **35**, 339–351 (2015).

[7] F.I.M. Ali, F. Awwad, Y.E. Greish, S.T. Mahmoud, Hydrogen sulfide ($H_2S$) gas sensor: A review. IEEE Sensors Journal, **19**(7), 2394–2407 (2018).

[8] P. Baldez, S. Fellows, R.E. Blakeley, *et al*., Measurements of 252Cf fission product energy loss through thin silicon nitride and carbon foils, and comparison with SRIM-2013 and MCNP6.2 simulations. Nuclear Instruments and Methods in Physics Research Section B: Beam Interactions with Materials and Atoms, **456**, 142–147 (2019).

[9] M. Martschini, L.K. Fifield, M.B. Froehlich, *et al*., New and upgraded ionization chambers for AMS at the Australian National University. Nuclear Instruments and Methods in Physics Research Section B: Beam Interactions with Materials and Atoms, **438**, 141–147 (2019).

[10] D.J. Morrissey, B.M. Sherrill, M. Steiner, *et al*., Commissioning the A1900 projectile fragment separator. Nuclear Instruments and Methods in Physics Research Section B: Beam Interactions with Materials and Atoms, **204**, 90–96 (2003).

[11] A. Göök, W. Geerts, F.-J. Hambsch, S. Oberstedt, M. Vidali, Sh. Zeynalov, A position-sensitive twin ionization chamber for fission fragment and prompt neutron correlation experiments. Nuclear Instruments and Methods in Physics Research Section A: Accelerators, Spectrometers, Detectors and Associated Equipment, **830**, 366–374 (2016).

[12] S.K. Shaikh, V.V. Ganbavle, S.I. Inamdar, K.Y. Rajpure, Multifunctional zinc oxide thin films for high-performance UV photodetectors and nitrogen dioxide gas sensors. RSC Advances, **6**(31), 25641–25650 (2016).

[13] P.T. Törmä, J. Kostamo, H. Sipilä, *et al*., Performance and properties of ultra-thin silicon nitride x-ray windows. IEEE Transactions on Nuclear Science, **61**(1), 695–699 (2014).

[14] J.D. Segal, C.J. Kenney, L. Rozario, *et al*., Thin-entrance window sensors for soft X-rays at LCLS-II. 2018 IEEE Nuclear Science Symposium and Medical Imaging Conference Proceedings (NSS/MIC), 1–2 (2018).

[15] C. Li, F. Shahriarian, M.S. Goorsky, The characterization of $Al_2O_3$ and $TiO_2$ antireflection coatings with a novel X-Ray reflectivity method and other experimental techniques. 2015 IEEE 42nd Photovoltaic Specialist Conference (PVSC), 1–5 (2015).

[16] F. Lemarquis, T. Begou, A. Moreau, J. Lumeau, Broadband antireflection coatings for visible and infrared ranges. CEAS Space Journal, **11**, 567–578 (2019).

[17] H.S. Kim, S.H. Park, J.H. Ha, *et al*., Development of a beta gauge system for a fabric density measurement. Applied Radiation and Isotopes, **67**(7-8), 1213–1215 (2009).

[18] A.M. Costa, L.V.E. Caldas, Câmara de ionização de placas paralelas para radiação-X de radiografia convencional e mamografia. Radiologia Brasileira, **41**, 39–43 (2008).

[19] G.V. Brown, P. Beiersdorfer, R. Goddard, *et al*., Thin-window high-efficiency position sensitive proportional counter for the vacuum flat crystal spectrometers on the Lawrence Livermore National Laboratory electron beam ion trap. Review of Scientific Instruments, **72**(1), 1249–1249 (2001).

[20] M. Döbeli, C. Kottler, M. Stocker, *et al*., Gas ionization chambers with silicon nitride windows for the detection and identification of low energy ions. Nuclear Instruments and Methods in Physics Research Section B: Beam Interactions with Materials and Atoms, **219**, 415–419 (2004).

[21] A.M. Müller, M. Döbeli, M. Suter, H.-A. Synal, Performance of the ETH gas ionization chamber at low energy. Nuclear Instruments and Methods in Physics Research Section B: Beam Interactions with Materials and Atoms, **287**, 94–102 (2012).

[22] S.M. Mirabedini, H. Arabi, A. Salem, S. Asiaban, Effect of low-pressure $O_2$ and Ar plasma treatments on the wettability and morphology of biaxial-oriented polypropylene (BOPP) film. Progress in Organic Coatings, **60**(2), 105–111 (2007).

[23] J. Yang, J. Bei, S. Wang, Improving cell affinity of poly(D, L-lactide) film modified by anhydrous ammonia plasma treatment. Polymers for Advanced Technologies, **13**(3-4), 220–226 (2002).

[24] J. Casimiro, B. Lepoittevin, C. Boisse-Laporte, M.-G. Barthès-Labrousse, P. Jegou, F. Brisset, P. Roger, Introduction of primary amino groups on poly(ethylene terephthalate) surfaces by ammonia and a mix of nitrogen and hydrogen plasma. Plasma Chemistry and Plasma Processing, **32**, 305–323 (2012).

[25] S. Zheng, J. Li, Inorganic–organic sol-gel hybrid coatings for corrosion protection of metals. Journal of Sol-Gel Science and Technology, **54**, 174–187 (2010).

[26] M. Iotti, P. Fabbri, M. Messori, F. Pilati, P. Fava, Organic–inorganic hybrid coatings for the modification of barrier properties of poly(lactic acid) films for food packaging applications. Journal of Polymers and the Environment, **17**, 10–19 (2009).

[27] A. Zeng, M. Shrestha, K. Wang, V.F. Neto, B. Gabriel, Q.H. Fan, Plasma treated active carbon for capacitive deionization of saline water. Journal of Nanomaterials, **2017**(1), 1934724 (2017).

[28] I. Banerjee, S.K. Mahapatra, C. Pal, A.K. Sharma, A.K. Ray, Effect of plasma power on reduction of printable graphene oxide thin films on flexible substrates. Materials Research Express, **5**(5), 056405 (2018).

[29] M.H. Moosavi, M.R. Khani, B. Shokri, S.M. Hosseini, S. Shojaee-Aliabadi, L. Mirmoghtadaie, Modifications of protein-based films using cold plasma. International Journal of Biological Macromolecules, **142**, 769–777 (2020).

[30] V. Luque-Agudo, M. Hierro-Oliva, A.M. Gallardo-Moreno, M.L. González-Martín, Effect of plasma treatment on the surface properties of polylactic acid films. Polymer Testing, **96**, 107097 (2021).